PNAS RESEARCH ARTICLE | CELL BIOLOGY

The exostosin glycosyltransferase 1/STAT3 axis is a driver of breast cancer aggressiveness

Balakrishnan Solaimuthu[a], Anees Khatib[a], Mayur Tanna[a], Abdelrahman Karmi[a], Arata Hayashi[a], Areej Abu Rmaileh[a], Michal Lichtenstein[a], Suranjana Takoe[b], Mohit Kumar Jolly[c], and Yoav David Shaul[a,1]

Edited by Joan Massagué, Memorial Sloan Kettering Cancer Center, New York, NY; received October 10, 2023; accepted December 7, 2023

The epithelial–mesenchymal transition (EMT) program is crucial for transforming carcinoma cells into a partially mesenchymal state, enhancing their chemoresistance, migration, and metastasis. This shift in cell state is tightly regulated by cellular mechanisms that are not yet fully characterized. One intriguing EMT aspect is the rewiring of the proteoglycan landscape, particularly the induction of heparan sulfate proteoglycan (HSPG) biosynthesis. This proteoglycan functions as a co-receptor that accelerates cancer-associated signaling pathways through its negatively-charged residues. However, the precise mechanisms through which EMT governs HSPG biosynthesis and its role in cancer cell plasticity remain elusive. Here, we identified exostosin glycosyltransferase 1 (EXT1), a central enzyme in HSPG biosynthesis, to be selectively upregulated in aggressive tumor subtypes and cancer cell lines, and to function as a key player in breast cancer aggressiveness. Notably, ectopic expression of EXT1 in epithelial cells is sufficient to induce HSPG levels and the expression of known mesenchymal markers, subsequently enhancing EMT features, including cell migration, invasion, and tumor formation. Additionally, EXT1 loss in MDA-MB-231 cells inhibits their aggressiveness-associated traits such as migration, chemoresistance, tumor formation, and metastasis. Our findings reveal that EXT1, through its role in HSPG biosynthesis, governs signal transducer and activator of transcription 3 (STAT3) signaling, a known regulator of cancer cell aggressiveness. Collectively, we present the EXT1/HSPG/STAT3 axis as a central regulator of cancer cell plasticity that directly links proteoglycan synthesis to oncogenic signaling pathways.

breast cancer | epithelial-mesenchymal transition | heparan sulfate | exostosin glycosyltransferase 1 | STAT3 signaling

Significance

By executing the EMT program, cancer cells can shift to a more aggressive state, with enhanced migration and metastasis capabilities. However, the cellular mechanisms that regulate the EMT are not fully characterized. Here, we demonstrate the critical role of EXT1, a central enzyme in the heparan sulfate proteoglycan (HSPG) biosynthesis, in cancer aggressiveness. We observed that EXT1 upregulation correlates with aggressive tumor subtypes, and its ectopic expression significantly promotes cell migration, invasion, tumor formation, and STAT3 activation. Moreover, EXT1 knockout in aggressive cancer cell lines impaired their EMT-associated traits. Therefore, EXT1, through HSPG biosynthesis, modulates STAT3 signaling, suggesting the EXT1/HSPG/STAT3 axis as a key regulator of cancer cell plasticity.

In recent decades, significant advancements have been made in breast cancer diagnosis and treatment, improving patient outcomes. However, challenges such as tumor metastasis and drug resistance continue to hinder effective cancer therapy (1). The induction of the epithelial–mesenchymal transition (EMT) program represents a potential mechanism through which carcinomas acquire aggressive traits such as the initiation of the metastatic cascade and chemoresistance. Activation of this program triggers the transdifferentiation of carcinoma cells into a partially mesenchymal state (2), accompanied by profound changes in cellular physiology. These changes involve noticeable alterations in cell morphology, loss of cell–cell interactions (3), acquisition of migratory and invasive capabilities (4), development of chemoresistance (5), and remodeling of the proteoglycan landscape (6). Therefore, a deeper understanding of the cellular mechanisms mediating this program is crucial for advancing our comprehension of cancer biology and developing therapeutic strategies to impede its progression.

The extracellular matrix (ECM) plays a crucial role in cellular interactions and is enriched in proteoglycan (PG) and glycosaminoglycan (GSG), which form a complex network between cells (7). Among the PGs, heparan sulfate proteoglycans (HSPGs) are the most abundant (8) and ubiquitously expressed on the cell surface of diverse cell types, including tumors (9, 10). HSPGs are structurally comprised of repeating units of glucosamine and glucuronic acid (GlcA) (9), which are heavily modified with diverse sulfate groups (11), creating highly negatively-charged structures (10). This dynamic sulfation establishes highly critical binding sites for positively charged amino acids found in various soluble growth factors, cytokines, membrane proteins, and ECM components (12, 13). These interactions facilitate the binding of ligands to their respective receptors, triggering the activation of vital cancer-associated signaling pathways (14). However, the precise cellular mechanisms through which the EMT program regulates HSPG biosynthesis remain largely unexplored.

The synthesis of HSPGs is a complex and dynamic process orchestrated through a sequence of -reactions (15). These reactions include chain initiation, elongation, and

Author affiliations: [a]Department of Biochemistry and Molecular Biology, The Institute for Medical Research Israel-Canada, Faculty of Medicine, Hebrew University of Jerusalem, Jerusalem 9112001, Israel; [b]Department of Biological Sciences, Indian Institute of Science Education and Research, Berhampur 760010, India; and [c]Department of Bioengineering, Indian Institute of Science, Bangalore 560012, India

Author contributions: B.S. designed research; B.S., A. Khatib, M.T., A. Karmi, A.H., A.A.R., and M.L. performed research; A.H., S.T., and M.K.J. analyzed data; and B.S. and Y.D.S. wrote the paper.

The authors declare no competing interest.

This article is a PNAS Direct Submission.

Copyright © 2024 the Author(s). Published by PNAS. This article is distributed under Creative Commons Attribution-NonCommercial-NoDerivatives License 4.0 (CC BY-NC-ND).

[1]To whom correspondence may be addressed. Email: yoav.shaul@mail.huji.ac.il.

This article contains supporting information online at https://www.pnas.org/lookup/suppl/doi:10.1073/pnas.2316733121/-/DCSupplemental.

Published January 12, 2024.

subsequent modification (16), which occurs within the Golgi apparatus (17). The synthesis is mediated by the exostosin family, a group of type II transmembrane proteins, which includes five members: exostosin glycosyltransferase 1 (EXT1), EXT2, and three EXT-like proteins (EXTL1, EXTL2, and EXTL3) (18). These EXT-like enzymes catalyze the initial chain elongation step, adding β1,4-linked N-acetylgalactosamine (GalNAc) to the growing HS backbone (18). EXT1 and EXT2 form a stable complex essential for adding various repeating units of GlcNAc and GlcA to the initial chain (19, 20). The importance of these enzymes to HS synthesis is evidenced by EXT1 or EXT2 mutations, resulting in hereditary multiple exostoses (HME) (21). HME is a rare skeletal disorder characterized by multiple bony protuberances called exostoses, which can potentially progress into malignant chondrosarcoma (22, 23).

In this study, we unveiled that EXT1, through its pivotal role in HSPG biosynthesis, is a crucial regulator of the epithelial–mesenchymal transition (EMT) program. Furthermore, we established a direct correlation between EXT1 expression and aggressive cancer phenotypes associated with EMT. We found that EXT1 contributes to cancer progression by regulating the Janus kinase (JAK)-signal transducer and activator of transcription 3 (STAT3) pathway (8), a signaling cascade central to cell migration (24). Consequently, this study highlights the significance of the EXT1/HSPG/STAT3 axis as a central regulator of tumor progression, shedding light on the potential role of EXT1 as both a diagnostic marker and a therapeutic target for aggressive breast cancers.

Results

EXT1 Expression and Heparan Sulfate Levels Correlate with Breast Cancer Aggressiveness. We set out to determine whether the extracellular heparan sulfate proteoglycan (HSPG) landscape in breast cancer is subtype-dependent. Hence, we stained different breast-cancer-derived cell lines with the specific heparan sulfate antibody (10E4) (25) and found that mesenchymal cell lines (MDA-MB-231, MDA-MB-157, and Hs-578-T) exhibited significantly higher levels of HSPG compared to epithelial (MDA-MB-468, ZR-75-1, and MCF-7) (Fig. 1*A*). To rule out any cell-line–specific effects, we stained the immortalized human mammary epithelial (HMLE) cells (26) and their naturally occurring mesenchymal-derived cells (NAMEC) (27) with 10E4. We found that similarly to the breast cancer cell lines, NAMEC cells showed significantly elevated HSPG levels compared with their HMLE parental cells (Fig. 1*B*). Finally, to verify the specificity of the 10E4 antibody, we enzymatically cleaved the HS polysaccharides using heparinase III (28), resulting in a dose-dependent decrease in the percentage of 10E4-positive MDA-MB-231 cells (*SI Appendix*, Fig. S1*A*). Our findings indicate that the HSPG landscape correlates with the cell state, suggesting a cellular mechanism that differentially regulates HSPG biosynthesis in breast cancer cells.

The 10E4 antibody recognizes the naive form of the HS chain (25) without targeting any particular modification. Thus, we hypothesized that the EMT program mainly regulates a component of the HS biosynthesis involved in chain initiation or elongation rather than the modification step (17). The HSPG chain initiation step comprises eight distinct enzymes, whereas the chain elongation includes only EXT1 and EXT2 (*SI Appendix*, Fig. S1*B*). Previously, we classified cancer cell lines from the MERAV database (https://merav.wi.mit.edu/) (29) based on their transcriptomes into epithelial (378 cell lines) and mesenchymal (150 cell lines) (30). By analyzing the expression profile of the 10 HSPG biosynthesis genes between epithelial and mesenchymal cell lines, we found that eight were significantly upregulated in mesenchymal cells (*SI Appendix*, Fig. S1*C*). Among them, EXT1 exhibited the highest expression level in mesenchymal cells (Fig. 1*C* and *SI Appendix*, Fig. S1*C*), which we also identified in a recent study to be a mesenchymal metabolic signature (MMS) gene (30). Therefore, we focused on characterizing the role of EXT1's contribution to the EMT program and investigating its impact on cancer cell aggressiveness.

We confirmed that EXT1 expression is higher, at both the mRNA and protein levels, in mesenchymal breast cancer cell lines than in epithelial counterparts (Fig. 1*D* and *SI Appendix*, Fig. S2*A*). Given EXT1 upregulation in mesenchymal cell lines, we next set to determine whether the EMT program directly regulates its expression. We identified that in HMLE cells expressing Twist Family BHLH Transcription Factor 1 (Twist1) conjugated to estrogen receptor (HMLE-Twist-ER) (31), 4-hydroxytamoxifen (4-OHT) treatment for 15 d, upregulated EXT1 expression as well as other known mesenchymal markers such as vimentin (VIM) (Fig. 1*E*) and N-cadherin (*CDH2)* (*SI Appendix*, Fig. S2*B*). In addition, this treatment suppressed the expression of E-cadherin (ECAD), a known epithelial marker (Fig. 1*E* and *SI Appendix*, Fig. S2*B*). Furthermore, EXT1 exhibited a higher expression level in NAMEC than HMLE cells, in correspondence to the HSPG profile (Fig. 1*B*).

To demonstrate that these EMT-dependent changes in EXT1 expression are also present in breast-cancer–derived cell lines, we treated HCC1806, a triple-negative breast-cancer–derived cell line with the EMT inducer, transforming growth factor β1 (TGFβ1) (32). Similar to 4-OHT treatment in HMLE cells, TGFβ1 elevated EXT1 expression in HCC1806, which correlated with the known mesenchymal markers, vimentin (VIM), N-cadherin (NCAD), and fibronectin (FN) (Fig. 1*F*). Furthermore, by analyzing publicly available gene expression datasets, we established that the upregulation of EXT1 expression linked to EMT is not exclusive to breast cancers. Specifically, in three different non-small cell lung cancer (NSCLC) cell lines (A549, HCC827, and NCI-H358) treated with TGFβ1 for 3 wk (GSE49644) (33), we observed significant upregulation of EXT1 expression (*SI Appendix*, Fig. S2*C*). Finally, EXT1 expression levels correlated with the mesenchymal marker *CDH2* and showed an inverse correlation with the epithelial marker *CDH1*. Altogether, we determined that the EMT program is a central regulator of EXT1 expression in different cancer types.

Next, we investigated whether the correlation between EXT1 expression and mesenchymal markers extends to patient-derived cancer samples using the Gene ENrichment Identifier web-based tool (GENI, https://yoavshaul-lab.shinyapps.io/gsea-geni/) (34). GENI performed a Spearman's rank correlation coefficient analysis between *EXT1* expression and the whole transcriptome (~20,000 genes) of 25 cancer types, followed by gene set enrichment analysis (GSEA) (35). Interestingly, in all examined tumor types, this analysis demonstrated a significant correlation between *EXT1* expression and the EMT-associated hallmark gene set (Fig. 1*G* and *SI Appendix*, Fig. S2*D*). Then, we investigated breast cancer patient–derived samples to characterize EXT1 expression in the different subtypes. By analyzing two databases available on the cBioPortal (36), namely the cancer genome atlas (TCGA, PanCancer Atlas project) (37) and the molecular taxonomy of breast cancer international consortium (METABRIC) (38), we found that *EXT1* expression is significantly elevated in HER2 and basal compared to luminal A samples (*SI Appendix*, Fig. S2*E*). Additionally, tumor samples highly expressing EXT1 (EXT1-high) were significantly enriched with high-grade breast cancer subtypes, such as basal, claudin-low, and HER2, compared to EXT1-low samples (Fig. 1*H*). Moreover, by analyzing 45 human breast cancer tumor samples with an immunohistochemical assay for EXT1,

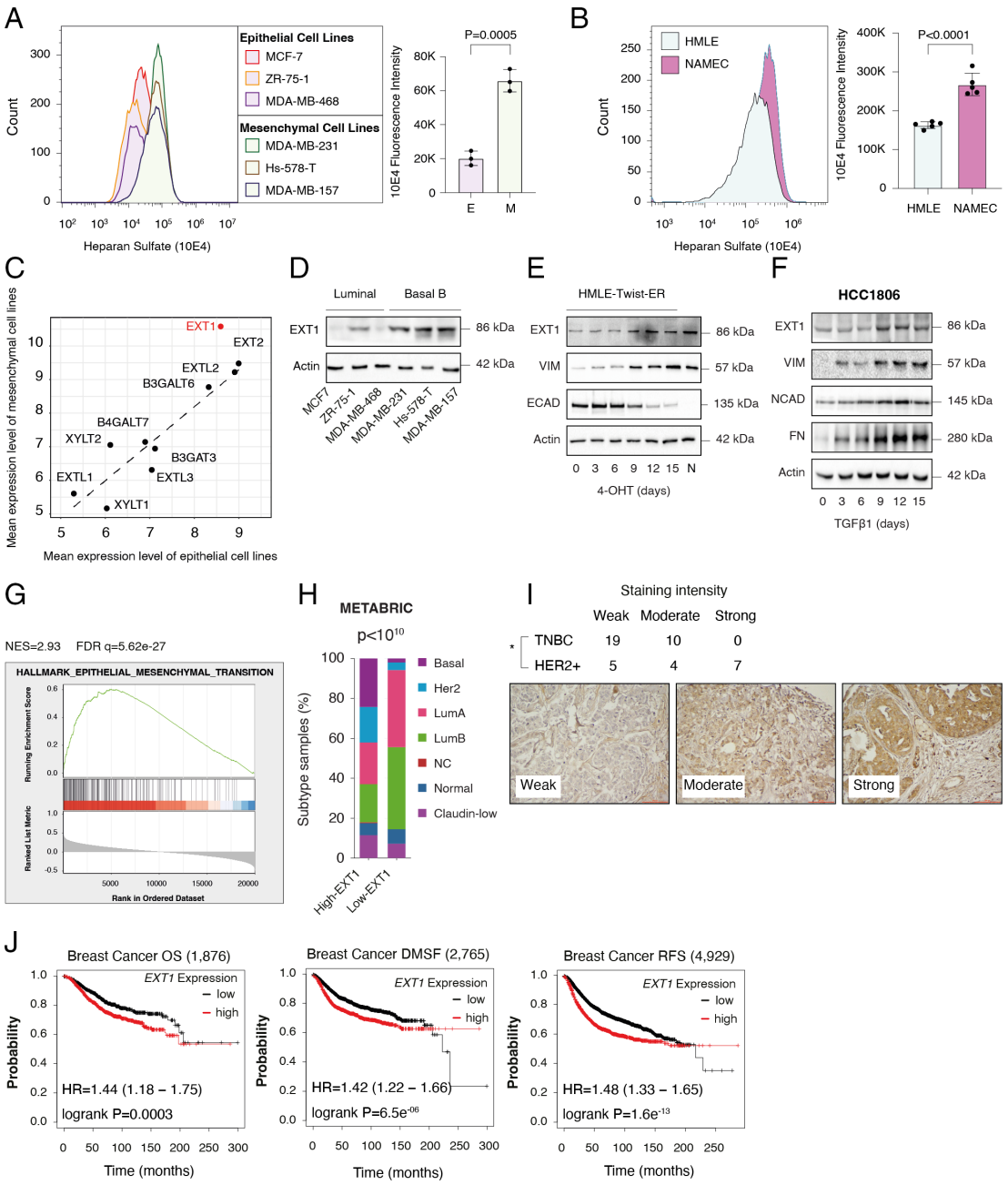

Fig. 1. EXT1 expression and heparan sulfate levels correlate with breast cancer aggressiveness. (*A*) HSPG levels are upregulated in mesenchymal cell lines. The indicated breast cancer–derived cell lines were subjected to FACS analysis using heparan sulfate-specific 10E4 antibody (*Left*). The HS median fluorescence intensity was calculated for the epithelial (E) and mesenchymal cell lines (M) (*Right*); each bar represents the mean ± SD for n = 3. The *P*-value was determined by Student's *t* test. (*B*) HSPG levels are upregulated in NAMEC vs. HMLE cells. NAMEC is an HMLE-derived cell line that spontaneously acquired the mesenchymal state. The indicated HMLE and NAMEC cell lines were subjected to FACS analysis using the indicated 10E4 antibody (*Left*). The HS median fluorescence intensity was calculated for the epithelial and mesenchymal cell lines (*Right*); each bar represents the mean ± SD for n = 5. The *P*-value was determined by Student's *t* test, (*C*) EXT1 demonstrated elevated expression in mesenchymal cells. Cancer cell lines were divided into epithelial (n = 378 cell lines) and mesenchymal (n = 150 cell lines) groups based on the expression of known mesenchymal markers. The expression of the 10 HS biosynthesis genes was compared with the mean expression in each group. The regression line is presented as a dashed line. (*D*) The EXT1 protein level is upregulated in mesenchymal breast cancer cell lines. Cells were lysed and subjected to immunoblotting using the indicated antibodies. (*E*) EXT1 expression is upregulated during the EMT program. HMLE-Twist-ER cells were treated with 4-hydroxytamoxifen (OHT) to induce EMT for 15 d. The cells were collected every 3 d, then lysed and subjected to immunoblotting using the indicated antibodies. N-NAMEC cells. (*F*) TGFβ1 induces EXT1 expression. HCC1806 cells were treated with 5 ng/mL of TGFβ1 to induce the EMT program for 15 d. Cells were collected and subjected to immunoblotting on each indicated day using the indicated antibodies. (*G*) EXT1 expression in breast cancer patients correlates with the hallmark of EMT. Breast cancer patients' gene expression data were generated by the TCGA (PanCancer Atlas project) and analyzed using the cBioPortal web tool (https://www.cbioportal.org). In these samples, the expression of EXT1 was compared to the whole transcriptome (~20,000 genes). The genes were then ranked based on the obtained Spearman's rank correlation coefficient followed and subjected to gene set enrichment analysis (GSEA). GSEA computed the normalized enrichment score (NES) and false discovery rate (FDR) values. (*H*) EXT1 expression is elevated in the aggressive breast cancer subtypes. Breast cancer samples were divided into groups based on high and low EXT1 expression (one SD above or below the mean). For each group, the percentage of breast cancer subtypes is color-coded. The breast cancer data was obtained from the METABRIC databases. The cBioPortal calculated the *P*-values. Lum = luminal. (*I*) A table reporting the number of human breast cancer samples with "weak," "moderate," and "strong" EXT1 staining from triple-negative breast cancer (TNBC) or HER2+, PR-, and ER- (HER2+). Representative staining intensities are shown in images. Magnification, 20×, *$P = 0.03$ as determined by Fischer's exact test. (*J*) EXT1 expression is associated with overall survival (OE), relapse-free survival (RFS), and DM-free survival (DMFS). Kaplan–Meier survival plots for patients with breast cancer were divided into high EXT1 expression ["high" (red)] and low ["low" (black)]. The numbers in parentheses indicate the total number of patients. These plots were generated by the Kaplan–Meier plotter website. The EXT1 (201995_at Affymetrix ID symbol) was used for all the analyses. The number of patients in each study is indicated in parentheses. The hazard ratio (HR) and the log-rank *P*-value (p) were determined by the analysis tool.

we identified that EXT1 correlates significantly with HER2 expression in the background of ER and progesterone receptor (PR) negative samples (Fig. 1*I*).

Finally, we utilized the Kaplan–Meier Plotter tool (https://kmplot.com/analysis/) (39, 40) and the cBioPortal to explore the association between EXT1 expression levels and patient outcomes in breast cancer. Remarkably, we found a significant correlation between high EXT1 expression and poor patient outcomes in terms of overall survival (OS), relapse-free survival (RFS), and distant metastasis-free survival (DMFS) (Fig. 1*J* and *SI Appendix*, Fig. S2*F*). Furthermore, upon analyzing the data based on grade and subtype, we observed that, in high-grade (grade 3), positive lymph node status, and HER2-positive patient–derived samples, high EXT1 expression levels were associated with worse overall survival compared to low expression (*SI Appendix*, Fig. S2*G*). Collectively, our findings demonstrate that EXT1 expression is elevated in aggressive breast cancer subtypes and correlates with mesenchymal markers, indicating a potential role in the EMT program.

EXT1 Is Sufficient to Induce the EMT Program. Having established a direct correlation between EXT1 expression, HSPG levels, and cancer aggressiveness, we investigated the impact of manipulating EXT1 expression on HSPG biosynthesis and the EMT program. Accordingly, we ectopically expressed a FLAG-tagged EXT1 (EXT1-FLAG) in the breast cancer–derived epithelial cell lines MCF-7 and MDA-MB-468 (Fig. 2*A*), which exhibited relatively low endogenous EXT1 levels (Fig. 1*D*). By staining these two cell lines with 10E4, followed by FACS analysis, we observed a significant elevation in HSPG levels in cells expressing EXT1-FLAG (Fig. 2*B*). Then, to systematically assess the effect of EXT1 on cell physiology, we conducted a comparative RNA-seq analysis between wild-type MCF-7 (VC) and EXT1-FLAG cells (*SI Appendix*, Fig. S3*A* and Dataset S1). We ranked the genes based on their expression ratio and performed GSEA, which identified that EXT1 expression is sufficient to induce the hallmarks of the EMT gene set (Fig. 2*C*).

Next, we validated the GSEA results by individually examining the expression pattern of selected EMT markers. Specifically, we found that overexpressing EXT1 in MCF-7 cells is sufficient to induce known mesenchymal markers, including zinc finger protein SNAI1 (SNAIL), Fibronectin (FN), cluster of differentiation 44 (CD44), glutathione peroxidase 8 (GPX8), Zinc Finger E-and Box Binding Homeobox 1 (ZEB1) (Fig. 2*D* and *SI Appendix*, Fig. S3*B*), and zinc finger protein SLUG (Fig. 2*E*). Furthermore, in MDA-MB-468 cells, overexpression of EXT1 induced the mesenchymal markers vimentin (VIM), N-cadherin (NCAD), CD44, and GPX8 (Fig. 2 *D* and *F* and *SI Appendix*, Fig. S3*B*). Interestingly, in both cell lines, EXT1 overexpression down-regulated E-cadherin (ECAD) a known epithelial marker (Fig. 2 *D* and *E* and *SI Appendix*, Fig. S3*B*). In contrast, the catalytically inactive mutant form of EXT1 (EXT1-D164A-FLAG) (21) failed to elevate the HSPG level (Fig. 2*B*) and the expression of these mesenchymal genes in both cell lines (*SI Appendix*, Fig. S3*B*). In conclusion, our findings provide crucial insights into the role of EXT1 and its catalytic activity in modulating mesenchymal gene expression, shedding light on the connection between HSPG biosynthesis and the EMT program.

EXT1 Is a Potent Inducer of Cell Migration and Tumor Formation. Following the observation that EXT1 overexpression is sufficient to increase HSPG synthesis and induce EMT markers' expression in breast cancer–derived epithelial cells, we sought to investigate whether this enzyme also impacts the cell migratory capabilities. Utilizing the Incucyte Live-Cell analysis system, we found that EXT1 overexpression (EXT1-FLAG) significantly enhanced MDA-MB-468 cells' ability to close the wound (Fig. 3*A* and *SI Appendix*, Fig. S3*C*). Additionally, ectopic EXT1-FLAG expression in MCF-7 and MDA-MB-468 increased the cells' migratory (Fig. 3*B* and *SI Appendix*, Fig. S3*D*) and invasive capabilities (Fig. 3*C* and *SI Appendix*, Fig. S3*E*). Importantly, we found that the proliferation rate of EXT1-FLAG in both cells is relatively slower than in the control (*SI Appendix*, Fig. S3*F*). This reduction in the proliferation rate is one of the hallmarks of the EMT program (41), which supports the EXT1-dependent shift to a more mesenchymal state.

To further establish that the EXT1 overexpression effect on cell migration is mediated by HSPG synthesis, we overexpressed the catalytically inactive form of EXT1 (EXT1-D164A-FLAG). We found that overexpression of this mutation, as opposed to the WT form, fails to enhance the cell migratory capabilities (Fig. 3 *A–C* and *SI Appendix*, Fig. S3 *C–E*). Additionally, the treatment of MDA-MB-468 cells overexpressing EXT1 (EXT1-FLAG) with heparinase III significantly inhibited the migratory ability of these cells (*SI Appendix*, Fig. S3*G*). Collectively, we demonstrated that EXT1 per se is sufficient to increase the epithelial cell migratory capability via its role in HSPG synthesis.

To evaluate the impact of EXT1 on tumor formation, we injected luciferase and GFP-labeled (42) MDA-MB-468 cells overexpressing VC, EXT1-FLAG, or EXT1-D164A-FLAG, into the mammary fat pad of female NOD-SCID mice. Through monitoring the luciferase activity over 12 wk, we identified that EXT1 significantly increased tumor growth kinetics (Fig. 3*D*), size (Fig. 3 *E* and *F* and *SI Appendix*, Fig. S3*H*), and weight (Fig. 3*G*) compared to VC or the mutant. These findings collectively emphasize that the ectopic expression of enzymatically active EXT1 in epithelial cells leads to enhanced HSPG formation, consequently augmenting their migratory and tumor formation capabilities.

EXT1 is a Regulator of Breast Cancer Aggressiveness. After determining that ectopic expression of EXT1 is sufficient to induce HSPG formation and the EMT program, we took the opposite approach and investigated whether silencing EXT1 in mesenchymal cells would inhibit their aggressive characteristics. Hence, we utilized the CRISPR-Cas9 system to knockout EXT1 in the basal B breast cancer cell line, MDA-MB-231 (EXT1-KO) (Fig. 4*A*), resulting in substantial changes in cell morphology (Fig. 4*B*) and a significant reduction in HSPG levels (Fig. 4*C*), without impacting the proliferation rate (*SI Appendix*, Fig. S4*A*). To exclude any potential off-target effects, we introduced the wild-type EXT1 (EXT1-FLAG) or the catalytically inactive mutant (EXT1-D164A-FLAG) into the EXT1 knockout background. We found that while the ectopic expression of the wild-type form led to a notable increase in HSPG levels, the catalytically inactive mutant failed to induce proteoglycan synthesis (Fig. 4*C*).

To investigate the correlation between EXT1 loss, HSPG reduction, and cell migration, we utilized the Incucyte Live-Cell analysis system. We found a significant decrease in the wound healing kinetics of EXT1-KO cells compared to WT (EXT1-WT) (Fig. 4*D* and *SI Appendix*, Fig. S4*B*). Additionally, the loss of EXT1 (EXT1-KO) impaired the migratory and invasive capabilities of MDA-MB-231 cells (Fig. 4*E* and *SI Appendix*, Fig. S4*C*). Interestingly, while the WT form rescued the knockout effects, the catalytically inactive mutant failed to restore migratory and invasive abilities, underscoring the essential role of EXT1 enzymatic activity and, subsequently, HSPG synthesis in cell migration. Furthermore, we demonstrated that EXT1 loss sensitizes the cells to known anticancer drugs, such as 5-fluorouracil (5-FU),

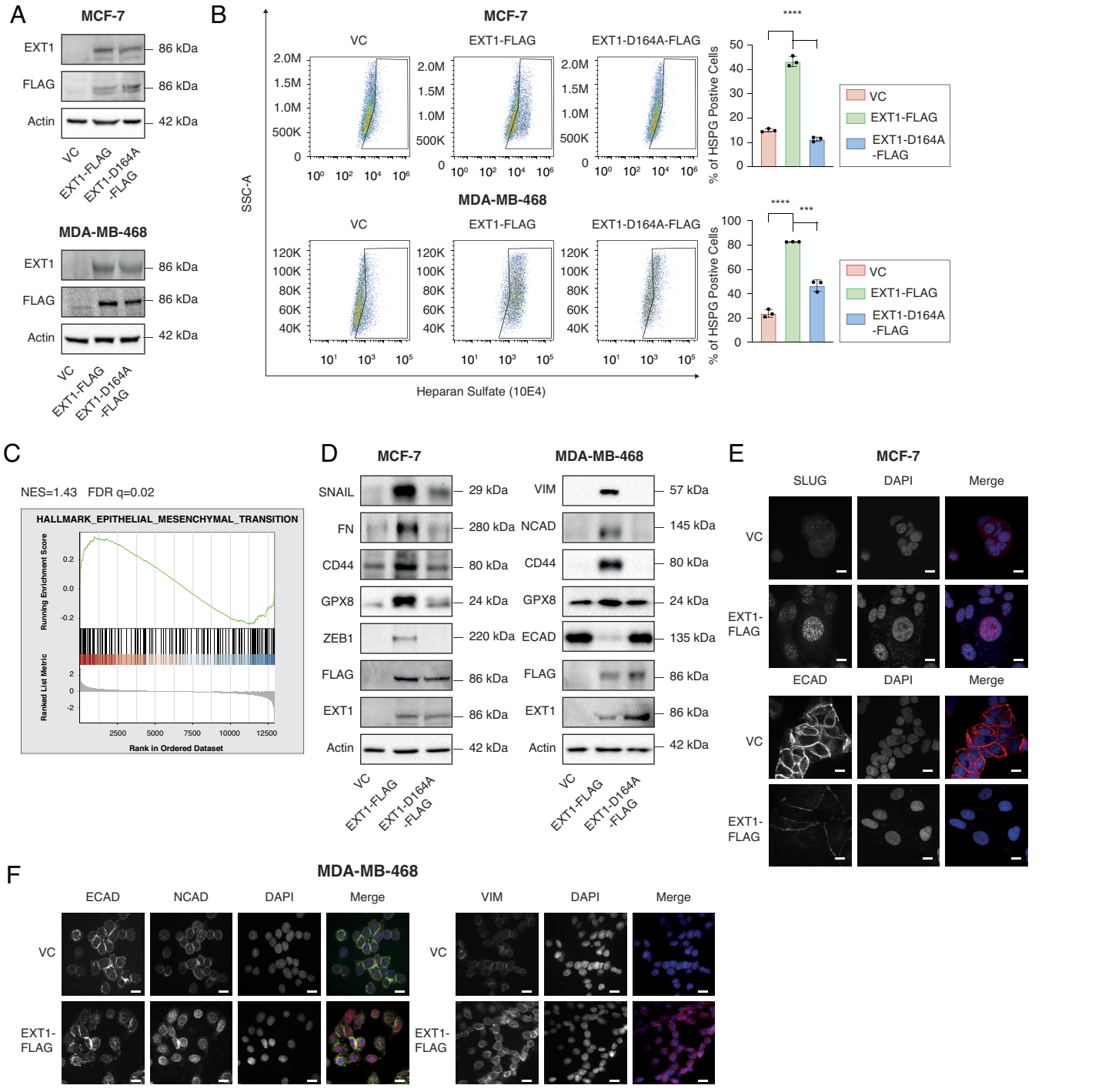

Fig. 2. EXT1 is sufficient to induce HSPG synthesis and the EMT program. (*A*) Immunoblots representing WT (VC), EXT1 overexpression (EXT1-FLAG), and the catalytically inactive mutant (EXT1-D164A-FLAG) in MCF-7 (*Upper*) and MDA-MB-468 (*Lower*) cancer cell lines. Cells were lysed and subjected to immunoblotting using the indicated antibodies. VC-vector control. (*B*) EXT1 activity is essential for HSPG formation. The same cells as (*A*) were subjected to FACS analysis using the indicated 10E4 antibody (*Left*). The HS median fluorescence intensity was calculated for each cell line (*Right*); each bar represents the mean ± SD for n = 3. $P = 0.0002$, $^{****}P < 0.0001$ was determined by Student's *t* test. (*C*) EXT1 induces the overexpression of the mesenchymal gene set. MCF-7 cells expressing vector control (VC) WT and EXT1-FLAG were subjected to comparative RNA-Seq analysis. For each gene, the ratio between WT and EXT1-FLAG was calculated, ranked, and then subjected to gene set enrichment analysis (GSEA). GSEA computed the normalized enrichment score (NES) and false discovery rate (FDR) values. (*D*) Selected EMT markers are upregulated in EXT1-FLAG expression in both MCF-7 and MDA-MB-468 breast cancer cell lines. Immunoblots representing WT (VC), EXT1 overexpression (EXT1-FLAG), and the catalytically inactive mutant (EXT1-D164A-FLAG) in MCF-7 (*Left*) and MDA-MB-468 (*Right*) cancer cell lines. Cells were lysed and subjected to immunoblotting using the indicated antibodies. VC-vector control. (*E*) EXT1 overexpression in MCF-7 affects SLUG and E-cadherin expression. EXT1-WT and EXT1-FLAG MCF-7 cells were subjected to immunofluorescence imaging using the indicated antibodies. ECAD = E-cadherin. (Scale bar: 10 μm.) (*F*) EXT1 overexpression in MDA-MB-468 affects E-cadherin (ECAD), N-cadherin (NCAD), and vimentin (VIM) expression. EXT1-WT and EXT1-FLAG MDA-MB-468 cells were subjected to immunofluorescence imaging using the indicated antibodies. (Scale bar: 10 μm.)

cyclophosphamide, and gemcitabine (Fig. 4*F*). These results demonstrate that EXT1 is vital for maintaining cellular mesenchymal features, such as migration ability and chemoresistance.

To exclude any cell line–specific effects, we also knocked out EXT1 in Hs-578-T (*SI Appendix*, Fig. S4*D*), another basal B breast cancer cell line. We found that similar to the MDA-MB-231 cell,

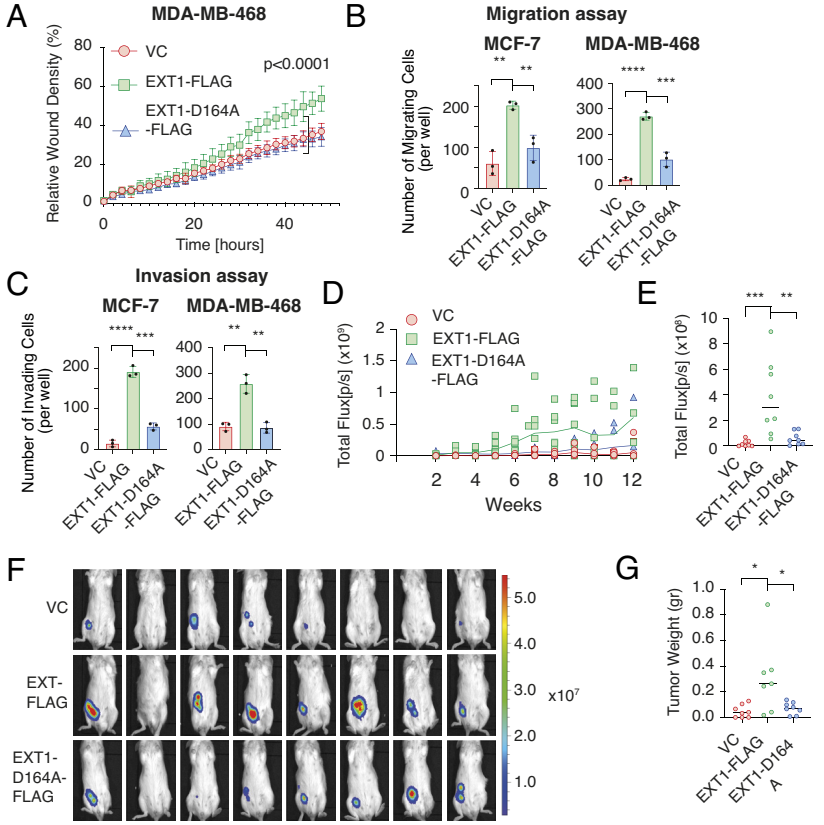

Fig. 3. EXT1 overexpression increases the epithelial cell migratory capabilities. (*A*) Real-time quantification of relative wound density for the indicated WT, EXT1-FLAG, and EXT1-D164A-FLAG cells. The cells were monitored for the indicated time. Each bar represents the mean ± SD for n = 8. The *P*-value was determined by Student's *t* test. (*B*) EXT1 overexpression induces MCF-7 and MDA-MB-468 cell migration. The migratory capability of the different samples was determined in a Boyden chamber-based transwell migration assay. Quantification of data is reported as the number of migrated cells per 25,000 seeded cells; each bar represents the mean ± SD for n = 3. $^{**}P = 0.0013$ (*Left*) $P = 0.0052$ (*Right*), $^{***}P = 0.0008$, $^{****}P < 0.0001$ was determined by Student's *t* test. (*C*) EXT1 overexpression induces MCF-7 and MDA-MB-468 cell invasion. The indicated cells were infected and treated as in (*B*), and the number of the Matrigel-invading cells was measured. Quantification of data is reported as the number of invading cells per 20,000 seeded cells; each value represents the mean ± SD for n = 3. $^{**}P = 0.002$, $^{***}P = 0.0001$, $^{****}P < 0.0001$ was determined by Student's *t* test. (*D*) EXT1 expression increases the tumor growth kinetics. MDA-MB-468 cells were injected into the mammary fat pad in SCID/NOD mice. At the indicated week, the tumor growth kinetics of WT MDA-MB-468 (VC), EXT1-FLAG, and EXT1-D164A-FLAG overexpressing cells in NOD-SCID mice were determined every 2 wk by the bioluminescence machine. (*E*) Quantification of the bioluminescence images. Each sphere represents the bioluminescence in a mouse n = 8. $^{**}P = 0.003$, $^{***}P = 0.0003$ was determined by the Mann-Whitney *U* test. (*F*) Representative images of NOD-SCID mice after 12 wk post-injection with MDA-MB-468 cells expressing VC, EXT-FLAG, or EXT1-D164A-FLAG were captured using bioluminescence. The color bar represents the intensity of luminescence. (*G*) The tumors were harvested from the mice, weighed, and presented as a graph. $^{*}P = 0.023$ (*Left*) $P = 0.037$ (*Right*) was determined by Student's *t* test.

EXT1 loss in Hs-578-T (EXT1-KO) reduced the expression of known EMT markers such as *CDH2*, *ZEB1*, *CD44*, *FN1*, *TWIST1*, *SNAI2*, and interleukin 6 (*IL-6*) (*SI Appendix*, Fig. S4*E*). Moreover, EXT1 loss in Hs-578-T (EXT1-KO) significantly diminished HSPG levels (*SI Appendix*, Fig. S4*F*) and the migratory ability of the cells (*SI Appendix*, Fig. S4*G*). Finally, we treated MDA-MB-231 cells with heparinase III, which substantially reduced the cells' migratory capacity (*SI Appendix*, Fig. S4*H*). Collectively, these findings support the crucial role of EXT1 as a regulator of cancer cell migration through its involvement in HSPG synthesis.

EXT1 Is Essential for Tumor Formation and Metastasis. We assessed the effect of EXT1 expression on tumor formation by injecting luciferase- and GFP-labeled MDA-MB-231 (EXT1-WT and EXT1-KO) cells into the mammary fat pad of female NOD-SCID mice. Tumor growth was continuously monitored for 8 wk using noninvasive bioluminescence imaging. We verified EXT1 knockout (*SI Appendix*, Fig. S5*B*) and found that these tumors, relative to WT, demonstrated a significantly slower growth rate (Fig. 5 *A* and *B*) and a substantial reduction in average tumor weight (Fig. 5*C* and *SI Appendix*, Fig. S5*A*). Next, we examined whether EXT1 knockout affects lung metastasis. We found that 6 out of 10 mice bearing MDA-MB-231 wild-type (EXT1-WT) cells xenograft demonstrated GFP-positive metastases within their lungs (Fig. 5 *D* and *E*). However, none was detected in those injected with EXT1-KO cells (*SI Appendix*, Fig. S5*C*). Next, due to the variation in tumor sizes obtained by the xenograft model, we sought to eliminate any bias in the metastasis formation by administrating an identical number of cells into the lateral tail vein of mice. We detected that after 4 wk, EXT1-WT and EXT1-KO+EXT1-FLAG cells formed GFP-positive colonies within their lungs (Fig. 5*F*). In contrast, cells lacking EXT1 expression (EXT1-KO) failed to form colonies, indicating the critical role of this enzyme in the metastatic cascade. In summary, these results highlight the pivotal function of the EXT1-HSPG axis in cancer aggressiveness, including cell migration, tumor growth, and metastasis.

EXT1 is a Vital Regulator of STAT3 Signaling. To elucidate the mechanisms underlying the role of EXT1 in breast cancer aggressiveness, we conducted a comparative CEL-Seq analysis (43) for wild-type (EXT1-WT) and knockout (EXT1-KO) MDA-MB-231 cells (Dataset S2), then we ranked the genes based on their expression ratio followed by GSEA. We revealed a significant reduction in 15 hallmarks (*SI Appendix*, Fig. S6*A*), including the

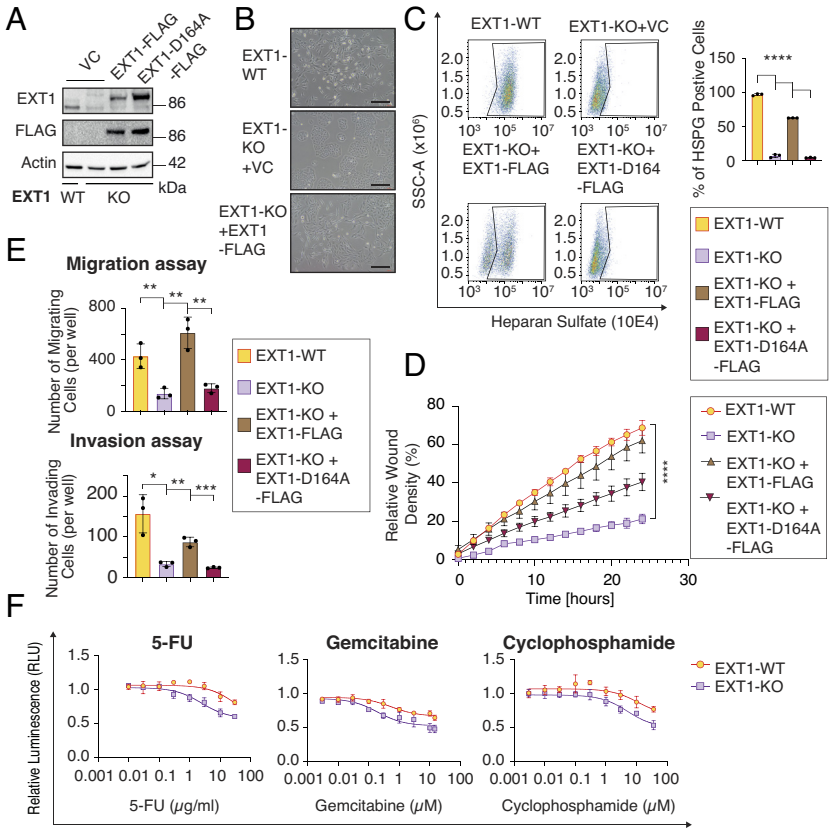

Fig. 4. EXT1 expression regulates breast cancer aggressiveness. (*A*) Immunoblot representing EXT1 knockout (EXT1-KO) in MDA-MB-231. EXT1 knockout was generated using the CRISPR-Cas9 system, followed by separating the cells into single clones. FLAG-tagged EXT1 (EXT1-FLAG) and catalytically inactive mutant (EXT1-D164A-FLAG) were reintroduced into EXT1-KO cells. Cells were lysed and subjected to immunoblotting using the indicated antibodies. (*B*) Silencing of EXT1 expression in MDA-MB-231 cells using the CRISPR-Cas9 system induces epithelial-like characteristics. (Scale bar: 100 μm.) (*C*) EXT1 activity is essential for HSPG formation. The same cells as (*A*) were subjected to FACS analysis using the indicated 10E4 antibody (*Left*). The HS median fluorescence intensity was calculated for each sample (*Right*). Each bar represents the mean ± SD for n = 3. ****$P < 0.0001$ was determined by Student's *t* test. (*D*) The same cells as (*A*) were subjected to real-time quantification of relative wound density. The cells were monitored for the indicated time. Each bar represents the mean ± SD for n = 8. ****$P < 0.0001$ was determined by Student's *t* test. (*E*) EXT1 loss inhibits cell migration and invasion in breast cancer cells. The same cells as (*A*) were subjected to Boyden chamber-based transwell migration assay (*Left*). Quantification of data is reported as the number of migrated cells per 20,000 seeded cells; each bar represents the mean ± SD for n = 3. The *P*-value was determined by Student's *t* test. The same cells as (*A*) were subjected to a Matrigel-based invasion assay (*Right*). Quantification of data is reported as the number of migrated cells per 25,000 seeded cells. Each value represents the mean ± SD for n = 3. *$P = 0.01$, **$P = 0.002$, ***$P = 0.0008$ was determined by Student's *t* test. (*F*) EXT1 loss induces drug sensitivity. EXT1-WT and EXT1-KO cells were treated with increasing concentrations of 5-fluorouracil (5-FU, *Top*), cyclophosphamide (*Middle*), and gemcitabine (*Bottom*). The cells were treated with the drugs for 48 h, then the number of cells was measured using CellTiter Glo. For each time point, n = 3.

"Hallmark of EMT" (NES, −1.46) (*SI Appendix*, Fig. S6*B*) as well as the "Hallmark of IL6 STAT3 Signaling," where the latter demonstrated the lowest normalized enrichment score (NES, −1.78) (Fig. 6*A* and *SI Appendix*, Fig. S6*C*). In addition to the GSEA, we identified that EXT1 loss reduced the expression of multiple cytokines, including IL-24, CSF2, and IL-6 (*SI Appendix*, Fig. S6*D*), which we verified using qPCR (*SI Appendix*, Fig. S6*E*) and ELISA for IL-6 (Fig. 6*B*). Thus, this bioinformatic analysis indicates that EXT1 participates in STAT3 signaling regulation.

To further validate the pivotal role of EXT1 as a regulator of STAT3 signaling cascade, we examined the correlation between EXT1 expression and STAT3 activation by detecting its phosphorylation at tyrosine 705 (Y705). We found a significant reduction in STAT3 phosphorylation levels in EXT1 knockout (EXT1-KO) compared to wild-type (EXT1-WT) MDA-MB-231 cells (Fig. 6*C*). Notably, reintroducing the wild-type EXT1 (EXT1-KO+EXT1-FLAG) but not the catalytically inactive mutant (EXT1-KO+EXT1-D164A-FLAG) restored STAT3 phosphorylation levels. Furthermore, ectopic expression of EXT1 in MCF-7 and MDA-MB-468 cells increased STAT3 phosphorylation levels (Fig. 6*D*). Moreover, tumors originating from MDA-MB-231 cells lacking EXT1 (EXT1-KO) exhibited lower STAT3 phosphorylation levels (Fig. 6*E* and *SI Appendix*, Fig. S6*F*) and its downstream target, vimentin (24) relative to EXT1-WT (*SI Appendix*, Fig. S6*G*). Whereas tumors originating from MDA-MB-468 cells ectopically expressing EXT1-FLAG exhibited higher STAT3 phosphorylation levels than those from WT or catalytically inactive mutant cells (Fig. 6*F*).

To demonstrate whether there is a clinical connection between EXT1 and STAT3 signaling, we analyzed TCGA pan-cancer atlas data (44) and tumor microarrays. we found a significant association between EXT1 expression and IL-6/JAK/STAT3 signaling (*SI Appendix*, Fig. S6*H*), which was supported by EXT1 staining (*SI Appendix*, Fig. S6*I*) that significantly correlated with vimentin (Spearman's correlation coefficient = 0.1734, *P*-value 0.02). Collectively, our findings indicate a strong association between EXT1 expression and STAT3 phosphorylation levels, suggesting that this enzyme plays an instructive role in this signaling cascade.

To elucidate the role of EXT1 in the JAK/STAT3 cascade, we employed Hyper-IL6 (45), a fusion protein comprising IL-6 and soluble IL6-receptor (sIL6R), known to activate STAT3 strongly (24). We found that Hyper-IL6 substantially induced STAT3 phosphorylation in WT cells, whereas it was attenuated in EXT1-KO cells (Fig. 6*G*). To further validate the EXT1/HSPG/STAT3 axis, we

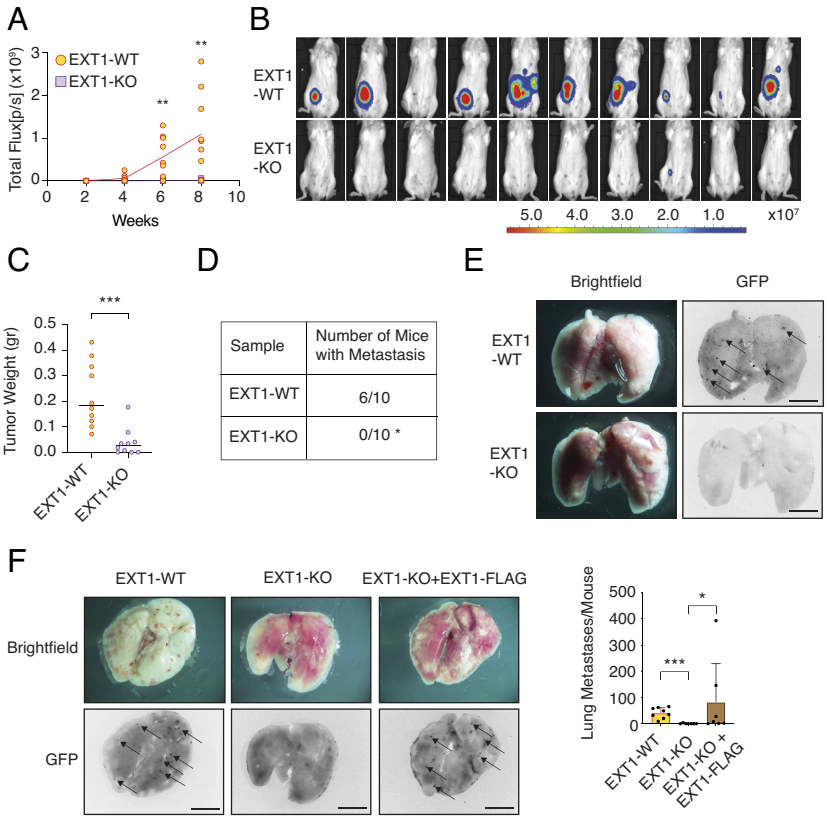

Fig. 5. EXT1 loss affects tumor formation and metastasis in mice. (*A*) The kinetics effect of EXT1 loss on tumor growth was determined by the bioluminescence machine. In vivo, tumor growth kinetics of WT MDA-MB-231 (EXT1-WT) and EXT1-KO cells were determined every 2 wk in NOD-SCID mice $^{**}P = 0.004$, the *P*-value was determined by Student's *t* test, n = 9. (*B*) Representative images of mice after 4 wk post-injection. The images were captured using bioluminescence. The color bar represents the intensity of luminescence. (*C*) The tumors were harvested from the mice, weighed, and presented as a graph. $^{***}P = 0.0005$ was determined by Student's *t* test, n = 9. (*D*) EXT1 loss inhibits metastasis formation. Female NOD-SCID mice were injected with EXT1-WT or EXT1-KO MDA-MB-231 cells. The table reports the number of mice with positive GFP colonies in their lung out of the total number of mice. $^{*}P = 0.01$ as determined by Fischer's exact test. (*E*) EXT1 loss reduces the number of lung metastases. Representative lungs were obtained from WT- and EXT1-KO-injected mice as described in (*A*). Brightfield images of the lung (*Left*). Fluorescence images of GFP-labeled colonies (*Right*). Arrows indicate the detected GFP-expressing metastases. (Bar: 5 mm.) (*F*) EXT1-WT, EXT1-KO, and EXT1-KO+EXT1-FLAG MDA-MB-231 cells were injected into the mouse tail vein for 4 wk. Representative lungs were obtained from the injected mice. Brightfield images of the lung (*Left*). Fluorescence images of GFP-labeled colonies (*Middle*). Arrows indicate the detected GFP-expressing metastases. (Bar: 5 mm.) The GFP-labeled colonies in the lung were quantified (*Right*). $^{*}P = 0.01$, $^{***}P = 0.0003$ was determined by the Mann-Whitney *U* test. Each bar represents the mean ± SD, EXT1-WT n = 8, other samples n = 7.

introduced a constitutively activated form of STAT3 (A662C, N664C, V667L, and CA-STAT3) (46) into EXT1-KO cells. Remarkably, in these knockout cells, CA-STAT3 significantly enhanced the expression of selected EMT markers and IL-6 (Fig. 6*H*) and increased the migratory capability (Fig. 6*I* and *SI Appendix*, Fig. S7*A*). Conversely, the treatment of MDA-MB-468 cells overexpressing EXT1 (EXT1-FLAG) with ruxolitinib (RUXO), a potent inhibitor of JAK1/2 (47), inhibited their STAT3 phosphorylation levels (*SI Appendix*, Fig. S7*B*), and attenuated their migration capabilities (Fig. 6*J* and *SI Appendix*, Fig. S7*C*). In addition, RUXO treatment reduced the migration capabilities of MDA-MB-231 cells (*SI Appendix*, Fig. S7*D*), linking STAT3 activation to cell migration. Finally, we determined the essentiality of HSPG to STAT3 signaling in MDA-MB-231 cells as heparinase III treatment, attenuated STAT3 phosphorylation levels (*SI Appendix*, Fig. S7*E*), linking HSPG formation to JAK/STAT3 activation. These findings demonstrate the essential function of EXT1 in cancer aggressiveness by governing cancer cell migration through its role in the HSPG/STAT3 axis.

Discussion

Our study has uncovered EXT1 as a central regulator of breast cancer aggressiveness through its involvement in HSPG synthesis. By analyzing patient-derived databases, we demonstrated that EXT1 expression is upregulated in high-grade breast cancer subtypes, such as HER2-positive, and was associated with poor prognosis. Moreover, we showed that EXT1 expression is induced by the EMT program, further emphasizing its relevance in cancer progression. To establish the essential role of EXT1 in breast cancer aggressiveness, we manipulated its expression level and assessed its impact on cellular physiology. Specifically, we showed that ectopic expression of EXT1 in epithelial cell lines induced HSPG synthesis and, subsequently, their capability to migrate, invade, and initiate tumors in mice. In contrast, EXT1 knockout in the highly aggressive MDA-MB-231 mesenchymal-like breast cancer cell line reduces HSPG level, migratory and invasion capabilities, tumor initiation abilities, and metastasis. Additionally, EXT1 loss inhibited the JAK/STAT3 signaling cascade, a central regulator of cancer cell aggressiveness (Fig. 6*K*). These findings unveil an EXT1/HSPG /STAT3 axis that regulates cellular migration and thus provides a direct link between metabolic enzymes synthesizing proteoglycans and oncogenic signaling pathways.

Syndecans and glypicans are the prominent families of cell surface proteins that undergo modification by HS (15). The syndecan family comprises four members (SDC1-4) (8), with syndecan-1 (SDC1, CD138) expressed in various tissues and tumors, including breast cancers (48). In breast cancers, SDC1 has been implicated in promoting tumor growth, invasion, metastasis, and chemoresistance (12, 49) and is significantly associated with poor

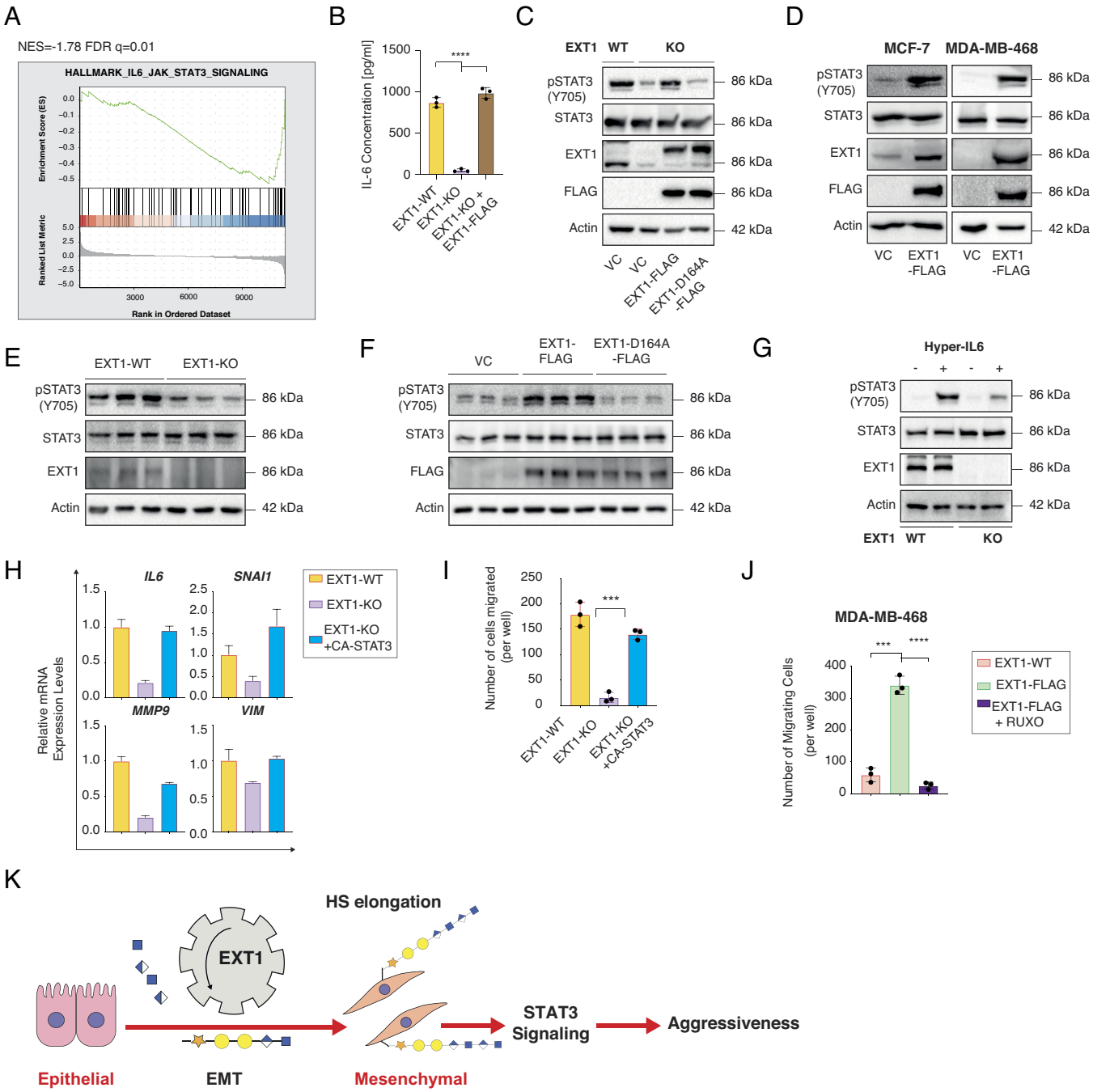

Fig. 6. EXT1 loss impairs STAT3 signaling. (*A*) EXT1 loss reduces the gene expression pattern for "hallmark IL-6/JAK/STAT3 signaling." MDA-MB-231 WT cells and EXT1-KO-1 were subjected to CEL-Seq analysis. The expression ratio of all genes was calculated and ranked based on the relative expression in EXT1-WT and EXT1-KO. The samples were subjected to GSEA. The FDR q-value was computed by GSEA. (*B*) IL-6 level is reduced in EXT1-KO cells growth media. After 36 h, cell growth media was collected from each indicated sample, and the IL-6 level was measured using a specific ELISA kit. ****$P < 0.0001$ was determined by Student's *t* test, n = 3. (*C*) STAT3 phosphorylation correlates with EXT1 expression. Immunoblots representing WT MDA-MB-231 expressing VC, EXT1 knockout (EXT1-KO), and overexpression of the full-length variant (EXT1-FLAG) or the catalytically inactive mutant (EXT1-D164A-FLAG) in the KO background. Cells were lysed and subjected to immunoblotting using the indicated antibodies. (*D*) EXT1 overexpression in epithelial MCF-7 and MDA-MB-468 cell lines induces STAT3 signaling. Cells expressing vector control (VC) and EXT1-FLAG were lysed and subjected to immunoblotting using the indicated antibodies. (*E*) Tumors generated from MDA-MB-231 cells that lack EXT1 expression (EXT1-KO) demonstrated reduced STAT3 phosphorylation levels. Three representative tumors originating from WT or EXT1-KO cells were lysed and subjected to immunoblotting using the indicated antibodies. (*F*) Tumors generated from MDA-MB-468 cell ectopically expressing EXT1-FLAG cells demonstrated elevated STAT3 phosphorylation. Three representative tumors originating from vector control (VC), EXT1-FLAG, or EXT1-D164A-FLAG cells were lysed and subjected to immunoblotting using the indicated antibodies. (*G*) Loss of EXT1 expression results in STAT3 signaling inhibition. EXT1-WT and EXT1-KO cells were starved with 0% FBS medium for 16 h and treated with 0 and 50 µL of media from HEK-293 cells generating Hyper IL-6 for 1 h. Cells were subjected to immunoblot using the indicated antibodies. (*H*) CA-STAT3 induces EMT marker expression in MDA-MB-231 cells. RNA was isolated from WT, EXT1-KO, and EXT1-KO + CA-STAT3 cells, and the relative mRNA expression level of the indicated genes was determined by qRT-PCR. Each value represents the mean ± SD for n = 3. (*I*) Constitutively activated STAT3 (CA-STAT3) improves the migration of EXT1-KO cells. The migratory capability of the different samples was determined using a Boyden chamber-based transwell assay. Quantification of data is reported as the number of migrated cells per 20,000 seeded cells. Each bar represents the mean ± SD for n = 3. ***$P = 0.0001$ was determined by Student's *t* test. (*J*) Ruxolitinib (RUXO) inhibits EXT1-dependent migration. The indicated cells were subjected to a Boyden chamber-based transwell migration assay. Quantification of data is reported as the number of migrated cells per 20,000 seeded cells; each bar represents the mean ± SD for n = 3. ***$P = 0.0002$, ****$P < 0.0001$ was determined by Student's *t* test. (*K*) A schematic representation of the EXT1/HSPG/STAT3 axis in driving cancer cell aggressiveness.

patient prognosis (50). Moreover, previous studies have demonstrated that SDC1 silencing attenuates STAT3 signaling (13). Based on these findings, we speculate that many of the EXT1/HSPG-dependent cellular effects observed in our study may be mediated through SDC1.

The HS synthesis machinery involves the formation of hetero-oligomeric complexes between EXT1 and EXT2. These complexes exhibit significantly higher glycosyltransferase and polymerizing activities than each enzyme individually (19). Despite their similarities, studies have revealed physiological differences between EXT1 and EXT2. For example, in vitro experiments demonstrated that both enzymes cannot substitute for each other (19). Furthermore, Ext1 knockout mice are lethal during gastrulation, whereas Ext2-null mice develop normally until embryonic day 6.0 (22). Furthermore, analysis of the human gene mutation database (HGMD) indicates a higher frequency of causative alterations in EXT1 compared to EXT2 (23). Finally, patients with EXT1 mutations and multiple osteochondromas are more prone to malignant transformation than those with EXT2 mutations (51, 52). In our study, genetic manipulation techniques established a clear correlation between EXT1 and cancer cell aggressiveness, which was inert for endogenous EXT2 expression. These findings suggest that the failure of endogenous EXT2 to compensate for EXT1-dependent effects on cellular properties is attributed to their distinct and non-redundant features.

EXT1 has been implicated in various cancer types, highlighting its significance in disease progression and patient outcomes. For example, in acute lymphoblastic leukemia (ALL), EXT1 is identified as an indicator of NOTCH pathway activation (53). In hepatocellular carcinoma, improved disease-free survival is associated with high EXT1 mRNA levels (54). Whereas, in breast cancer, upregulation of EXT1 mRNA has been detected in estrogen receptor (ER)-negative cells (55) and proposed as a high-risk predictor for metastasis (56). Furthermore, EXT1 expression has been linked to cancer stemness in doxorubicin-resistant MCF-7 cells (MCF-7/ADR), where EXT1 promotes cancer stem cell properties (57). These studies collectively establish EXT1 as a marker of breast tumor aggressiveness. However, the underlying mechanisms by which EXT1 governs cell aggressiveness have remained elusive. In this study, we introduce the EXT1/HSPG/JAK/STAT3 axis, which unravels the mechanism through which EXT1 drives breast cancer cells toward a more aggressive state.

In a previous study, we employed a gene expression analysis combined with a FACS-based screen to identify a set of metabolic genes referred to as the "mesenchymal metabolic signature" (MMS), which showed potential involvement in regulating the EMT program (30). EXT1, together with dihydropyrimidine dehydrogenase (DPYD) and glutathione peroxidase 8 (GPX8), were the top hits in that screen (30). Since we demonstrated that all three enzymes are central regulators of the EMT program (30, 58), we validate the significance of that FACS-based screen and postulate that other hits contribute to tumor aggressiveness.

HSPGs comprise of highly sulfated repeating disaccharide units (59), present on the cell surface and in the extracellular matrix (6). Due to their negative charge, the sulfated chains act as co-receptors, enhancing the interactions between ligands and their respective receptors (60). This ligand–receptor interaction triggers the activation of the downstream signaling pathways, including MAPK, AKT, Wnt, and JAK/STAT3 (8, 60). Previous studies have demonstrated that reducing EXT1 expression levels results in shorter heparan sulfate (HS) chains (61). This decrease in HS chain length, caused by EXT1 loss, was reported to attenuate intracellular signaling, such as Wnt, in multiple myeloma cells (28). Our study aimed to unravel the cellular mechanisms by which EXT1 promotes breast cancer aggressiveness. Through unbiased CEL-Seq analysis followed by biochemical experiments, we identified the JAK/STAT3 signaling pathway as the primary pathway downregulated upon EXT1 loss. However, we cannot exclude the possibility that EXT1, through HSPG synthesis, also regulates other known signal transduction pathways. We focused on the JAK/STAT3 signaling cascade due to its pivotal role in regulating cancer cell aggressiveness (58) and migration (24).

In this study, we provide evidence highlighting the critical role of HSPG formation in breast cancer aggressiveness. The synthesis of HSPGs involves a series of sequential reactions (59) orchestrated by more than 20 different enzymes (15). Therefore, identifying potential targets within this metabolic pathway could have therapeutic implications. Furthermore, our findings demonstrate that ectopic expression of EXT1 alone is sufficient to induce HSPG formation, suggesting it has a pivotal regulatory role in this process. However, further investigations are needed to fully comprehend the underlying mechanisms by which EXT1 and heparan sulfate contribute to cancer aggressiveness and assess their translational potential. Overall, this study underscores the significance of the partially mesenchymal state in driving breast cancer aggressiveness and highlights the potential for targeting this state to develop effective therapeutic strategies.

Materials and Methods

Analysis of Breast Cancer Data in cBioPortal. The cBioPortal for Cancer Genomics is an open-access database providing visualization and analysis tools for large-scale cancer genomics datasets (https://cbioportal.org). For gene correlation analysis, we queried EXT1 in breast invasive carcinoma (TCGA, PanCancer Atlas project) or the METABRIC (containing 1,084 or 2,509 samples, respectively). Then, we subjected the genes to co-expression analysis and downloaded the correlation plots. For gene set enrichment analysis (GSEA), Spearman's rank correlation coefficient between the gene of interest and the whole genome was computed, downloaded, and subjected to GSEA and visualization of the result using the R package ClusterProfiler (62) and Enrichplot. For the different analyses, we selected the h.all.v7.2.symbole.gmt (Hallmarks) or C2.cp.kegg.v7.2.symbols.gmt (Curated) gene set databases. This analysis was conducted using the GENI web-based tool (https://yoavshaul-lab.shinyapps.io/gsea-geni/) (34).

Cancer Sample Analysis. KM analyses of the breast cancer samples were analyzed and generated by the KM Plotter website (https://kmplot.com/analysis/) (40). Search entries: EXT1 as the gene symbol (Affymetrix ID: 201995_at), the auto-select best cut-off for "split patients by." The obtained KM plots and the statistics were generated by the website. The breast cancer tissue microarray (TMA) (#BR881 and #BR1008b) was purchased from Tissuearray (USA). These samples were subsequently conducted to a 2-h baking process at 60 °C. The resulting slides were then utilized for immunohistochemistry, and pathologists carefully evaluated the staining intensity (0, 1, 2, and 3).

GEO Database Analysis. We downloaded high-throughput transcriptomics data of lung cancer cell lines treated with TGFβ1 and single-cell analysis from the GEO database. For the lung cancer datasets, we downloaded the samples from GSE49644 (33) and analyzed them using the custom probeset definition used for processing the arrays as defined by Dai et al. (63), so there was one probeset per Entrez Gene ID. For the single-cell RNA seq dataset, GSE147405 (64), the imputation of gene expression values was performed using MAGIC (65) before plotting the expression levels of EXT1. We used a two-tailed Student's *t* test under the assumption of unequal variances and computed significance for statistical comparison between discrete groups. Package matplotlib was used for plots. A two-tailed Student's *t* test with unequal variance was performed to compare between samples in discrete time groups. Error bars denoted the SD (statistical significance at $P < 0.05$).

Heparinase III Supplementation. Cells were seeded in 6 cm plates, and the next day, prior to experiments, the cells were washed with PBS twice and treated with Heparinase III (10 mU/mL) (6145-GH-010, Amsbio) diluted in DMEM or PBS for 1 h at 37 °C. After incubation, the cells are washed with PBS twice and subjected to respective experiments.

Animal Studies. MDA-MB-231 WT GFP$^+$ Luci$^+$ and EXT1-KO GFP$^+$ Luci$^+$ cells were injected into the mammary fat pad of female NOD-SCID mice (MDA-MB-231(1 × 10^6) cells. For overexpression, MDA-MB-468 WT, GFP$^+$ Luci$^+$, EXT1 OE GFP$^+$ Luci$^+$ and EXT1 OE-D164A GFP+ Luci$^+$ (5 × 10^6) cells per mouse). After the injection, the tumor growth kinetics were monitored in real-time using the noninvasive bioluminescence imaging system. We harvested the tumors and weighed them after 7 wk for mice injected with MDA-MB-231 or 12 wk for those injected with MDA-MB-468 cells. For tail vein injection, MDA-MB-231 WT GFP$^+$ Luci$^+$, EXT1-KO GFP$^+$ Luci$^+$, and EXT1-KO-Rescue GFP$^+$ Luci$^+$ (1 × 10^6) cells were injected into mice tail vein and allowed for 4 wk. All mouse experiments were conducted under The Hebrew University Institutional Animal Care and Use Committee-approved (IACUC) protocol MD-21-16429-5. In addition, the Hebrew University is certified by the Association for Assessment and Accreditation of Laboratory Animal Care (AAALAC). The metastatic GFP colonies were observed using the NIS Elements software package for multidimensional experiments and exported as 16-bit. The pictures were slightly adjusted (levels) using Adobe Photoshop.

Statistical Analysis. Data are shown as mean ± SD from at least three independent biological experiments. All statistical analyses were performed using the R (version 4.0) or GraphPad Prism (version 8.0) statistical analysis programs. If not indicated in the figure legend, all the *P*-values were calculated using the unpaired two-tailed Student's *t* test. Data distribution was assumed to be normal, but this was not formally tested. The significance of the mean comparison is present in each figure.

Data, Materials, and Software Availability. All study data are included in the article and/or supporting information.

ACKNOWLEDGMENTS. We thank the members of the Shaul laboratory. This work was supported by the Israel Science Foundation (Grant 1816/16 and 299/21), the Israel Cancer Research Fund project grant, and the Mizutani Foundation for Glycoscience (Grant # 220087). B.S. was supported by the Lady Davis Fellowship for postdoctoral researchers at The Hebrew University of Jerusalem. The Genomic Applications Laboratory of the Core Research Facility, The Faculty of Medicine, and The Hebrew University of Jerusalem, Israel, performed the RNA-Seq data analysis. We extend our gratitude to Prof. Eli Pikarsky of the Department of Pathology at Hadassah-Hebrew University Medical Center for his assessment of tissue array staining intensity. We are also grateful for the help of Prof. Zvi Granot from the Department of Developmental Biology and Cancer Research, Institute for Medical Research Israel Canada, Hebrew University Medical School, in conducting tail vein injections in mice. We thank Prof. Israel Voldavsky from the Israel Institute of Technology for his support and valuable suggestions.

1. M. Luo, M. Brooks, M. Wicha, Epithelial–mesenchymal plasticity of breast cancer stem cells: Implications for metastasis and therapeutic resistance. *Curr. Pharm. Design* **21**, 1301–1310 (2015).
2. E. D. Williams, D. Gao, A. Redfern, E. W. Thompson, Controversies around epithelial–mesenchymal plasticity in cancer metastasis. *Nat. Rev. Cancer* **19**, 716–732 (2019).
3. S. Brabletz, H. Schuhwerk, T. Brabletz, M. P. Stemmler, Dynamic EMT: A multi-tool for tumor progression. *Embo J.* **40**, e108647 (2021).
4. B. Bakir, A. M. Chiarella, J. R. Pitarresi, A. K. Rustgi, EMT, MET, plasticity, and tumor metastasis. *Trends Cell Biol.* **30**, 764–776 (2020).
5. F. Lüönd *et al.*, Distinct contributions of partial and full EMT to breast cancer malignancy. *Dev. Cell* **56**, 3203–3221.e11 (2021).
6. Z. Karagiorgou, P. N. Fountas, D. Manou, E. Knutsen, A. D. Theocharis, Proteoglycans determine the dynamic landscape of EMT and cancer cell stemness. *Cancers* **14**, 5328 (2022).
7. S. D. Vallet, O. Clerc, S. Ricard-Blum, Glycosaminoglycan–protein interactions: The first draft of the glycosaminoglycan interactome. *J. Histochem. Cytochem.* **69**, 93–104 (2020).
8. N. Hassan, B. Greve, N. A. Espinoza-Sánchez, M. Götte, Cell-surface heparan sulfate proteoglycans as multifunctional integrators of signaling in cancer. *Cell Signal* **77**, 109822 (2020).
9. J. O. S. Onyeisi, B. Z. F. Ferreira, H. B. Nader, C. C. Lopes, Heparan sulfate proteoglycans as targets for cancer therapy: A review. *Cancer Biol. Ther.* **21**, 1087–1094 (2020).
10. C. Marques, C. A. Reis, R. R. Vivès, A. Magalhães, Heparan sulfate biosynthesis and sulfation profiles as modulators of cancer signalling and progression. *Front. Oncol.* **11**, 778752 (2021).
11. J. D. Esko, S. B. Selleck, ORDER OUT OF CHAOS: Assembly of ligand binding sites in heparan sulfate1. *Annu. Rev. Biochem.* **71**, 435–471 (2002).
12. J. R. Couchman, Syndecan-1 (CD138), Carcinomas and EMT. *Int. J. Mol. Sci.* **22**, 4227 (2021).
13. S. A. Ibrahim *et al.*, Syndecan-1 is a novel molecular marker for triple negative inflammatory breast cancer and modulates the cancer stem cell phenotype via the IL-6/STAT3, Notch and EGFR signaling pathways. *Mol. Cancer* **16**, 57 (2017).
14. V. D. Pasquale, L. M. Pavone, Heparan sulfate proteoglycan signaling in tumor microenvironment. *Int. J. Mol. Sci.* **21**, 6588 (2020).
15. S. Sarrazin, W. C. Lamanna, J. D. Esko, Heparan sulfate proteoglycans. *Csh Perspect. Biol.* **3**, a004952 (2011).
16. F. E. Poulain, H. J. Yost, Heparan sulfate proteoglycans: A sugar code for vertebrate development? *Development* **142**, 3456–3467 (2015).
17. J.-P. Li, M. Kusche-Gullberg, Chapter six heparan sulfate: Biosynthesis, structure, and function. *Int. Rev. Cel Mol. Bio.* **325**, 215–273 (2016).
18. M. Busse-Wicher, K. B. Wicher, M. Kusche-Gullberg, The extostosin family: Proteins with many functions. *Matrix Biol.* **35**, 25–33 (2014).
19. C. McCormick, G. Duncan, K. T. Goutsos, F. Tufaro, The putative tumor suppressors EXT1 and EXT2 form a stable complex that accumulates in the Golgi apparatus and catalyzes the synthesis of heparan sulfate. *Proc. Natl. Acad. Sci. U.S.A.* **97**, 668–673 (2000).
20. M. Busse *et al.*, Contribution of EXT1, EXT2, and EXTL3 to heparan sulfate chain elongation*. *J. Biol. Chem.* **282**, 32802–32810 (2007).
21. P. K. Cheung *et al.*, Etiological point mutations in the hereditary multiple exostoses gene EXT1: A functional analysis of heparan sulfate polymerase activity. *Am. J. Hum. Genet.* **69**, 55–66 (2001).
22. D. Stickens, B. M. Zak, N. Rougier, J. D. Esko, Z. Werb, Mice deficient in Ext2 lack heparan sulfate and develop exostoses. *Development* **132**, 5055–5068 (2005).
23. E. Bukowska-Olech *et al.*, Hereditary multiple exostoses–a review of the molecular background, diagnostics, and potential therapeutic strategies. *Front. Genet.* **12**, 759129 (2021).
24. A. A. Rmaileh *et al.*, DPYSL2 interacts with JAK1 to mediate breast cancer cell migration. *J. Cell Biol.* **221**, e202106078 (2022).
25. G. David, X. M. Bai, B. V. der Schueren, J. J. Cassiman, H. V. den Berghe, Developmental changes in heparan sulfate expression: In situ detection with mAbs. *J. Cell Biol.* **119**, 961–975 (1992).
26. J. Yang *et al.*, Twist, a master regulator of morphogenesis, plays an essential role in tumor metastasis. *Cell* **117**, 927–939 (2004).
27. W. L. Tam *et al.*, Protein Kinase C α is a central signaling node and therapeutic target for breast cancer stem cells. *Cancer Cell* **24**, 347–364 (2013).
28. Z. Ren *et al.*, Syndecan-1 promotes Wnt/β-catenin signaling in multiple myeloma by presenting Wnts and R-spondins. *Blood* **131**, 982–994 (2018).
29. Y. D. Shaul *et al.*, MERAV: A tool for comparing gene expression across human tissues and cell types. *Nucleic Acids Res.* **44**, D560–D566 (2016).
30. Y. D. Shaul *et al.*, Dihydropyrimidine accumulation is required for the epithelial-mesenchymal transition. *Cell* **158**, 1094–1109 (2014).
31. S. A. Mani *et al.*, The epithelial-mesenchymal transition generates cells with properties of stem cells. *Cell* **133**, 704–715 (2008).
32. S. Kim, J. Lee, M. Jeon, S. J. Nam, J. E. Lee, Elevated TGF-β1 and -β2 expression accelerates the epithelial to mesenchymal transition in triple-negative breast cancer cells. *Cytokine* **75**, 151–158 (2015).
33. Y. Sun *et al.*, Metabolic and transcriptional profiling reveals pyruvate dehydrogenase kinase 4 as a mediator of epithelial-mesenchymal transition and drug resistance in tumor cells. *Cancer Metab.* **2**, 20 (2014).
34. A. Hayashi *et al.*, GENI: A web server to identify gene set enrichments in tumor samples. *Comput. Struct. Biotechnol. J.* **21**, 5531–5537 (2023), 10.1016/j.csbj.2023.10.053.
35. A. Subramanian *et al.*, Gene set enrichment analysis: A knowledge-based approach for interpreting genome-wide expression profiles. *Proc. Natl. Acad. Sci. U.S.A.* **102**, 15545–15550 (2005).
36. J. Gao *et al.*, Integrative analysis of complex cancer genomics and clinical profiles using the cBioPortal. *Sci. Signal* **6**, pl1–pl1 (2013).
37. G. Ciriello *et al.*, Comprehensive molecular portraits of invasive lobular breast cancer. *Cell* **163**, 506–519 (2015).
38. C. Curtis *et al.*, The genomic and transcriptomic architecture of 2,000 breast tumours reveals novel subgroups. *Nature* **486**, 346–352 (2012).
39. B. Győrffy *et al.*, An online survival analysis tool to rapidly assess the effect of 22,277 genes on breast cancer prognosis using microarray data of 1,809 patients. *Breast Cancer Res. Treatment* **123**, 725–731 (2010).
40. B. Győrffy, Survival analysis across the entire transcriptome identifies biomarkers with the highest prognostic power in breast cancer. *Comput. Struct. Biotechnol. J.* **19**, 4101–4109 (2021).
41. C. Blanpain, EMT transition states during tumor progression and metastasis. *Trends Cell Biol.* **29**, 212–226 (2019).
42. B. Solaimuthu, A. Hayashi, A. Khatib, Y. D. Shaul, Monitoring breast cancer growth and metastatic colony formation in mice using bioluminescence. *J. Vis. Exp.* **177** (2021), 10.3791/63060.
43. T. Hashimshony *et al.*, CEL-Seq2: Sensitive highly-multiplexed single-cell RNA-Seq. *Genome Biol.* **17**, 77 (2016).
44. K. A. Hoadley *et al.*, Cell-of-origin patterns dominate the molecular classification of 10,000 tumors from 33 types of cancer. *Cell* **173**, 291–304.e6 (2018).
45. M. Fischer *et al.*, A bioactive designer cytokine for human hematopoietic progenitor cell expansion. *Nat. Biotechnol.* **15**, 142–145 (1997).
46. C. A. Martz *et al.*, Systematic identification of signaling pathways with potential to confer anticancer drug resistance. *Sci. Signaling* **7**, ra121 (2014).
47. R. A. Mesa, Ruxolitinib, a selective JAK1 and JAK2 inhibitor for the treatment of myeloproliferative neoplasms and psoriasis. *Idrugs Investig. Drugs J.* **13**, 394–403 (2010).
48. S. A. Ibrahim *et al.*, Syndecan-1 (CD138) modulates triple-negative breast cancer stem cell properties via regulation of LRP-6 and IL-6-mediated STAT3 signaling. *Plos One* **8**, e85737 (2013).
49. M. R. Sayyad *et al.*, Syndecan-1 facilitates breast cancer metastasis to the brain. *Breast Cancer Res Tr* **178**, 35–49 (2019).
50. W. Qiao, H. Liu, W. Guo, P. Li, M. Deng, Prognostic and clinical significance of syndecan-1 expression in breast cancer: A systematic review and meta-analysis. *Eur. J. Surg. Oncol.* **45**, 1132–1137 (2019).
51. D. E. Porter *et al.*, Severity of disease and risk of malignant change in hereditary multiple exostoses. A genotype-phenotype study. *J. Bone Jt. Surg. Br.* **86**, 1041–6 (2004).
52. C. M. Alvarez, M. A. D. Vera, T. R. Heslip, B. Casey, Evaluation of the anatomic burden of patients with hereditary multiple exostoses. *Clin. Orthop. Relat. R* **462**, 73–79 (2007).
53. S. Daakour *et al.*, Systematic interactome mapping of acute lymphoblastic leukemia cancer gene products reveals EXT-1 tumor suppressor as a Notch1 and FBWX7 common interactor. *Bmc Cancer* **16**, 335 (2016).

54. S. Dong *et al.*, Increased EXT1 gene copy number correlates with increased mRNA level predicts short disease-free survival in hepatocellular carcinoma without vascular invasion. *Medicine* **97**, e12625 (2018).
55. S. Julien *et al.*, Selectin ligand Sialyl-Lewis x antigen drives metastasis of hormone-dependent breast cancers. *Cancer Res.* **71**, 7683–7693 (2011).
56. A. Taghavi *et al.*, Gene expression profiling of the 8q22-24 position in human breast cancer: TSPYL5, MTDH, ATAD2 and CCNE2 genes are implicated in oncogenesis, while WISP1 and EXT1 genes may predict a risk of metastasis. *Oncol. Lett.* **12**, 3845–3855 (2016).
57. S. Manandhar *et al.*, Exostosin 1 regulates cancer cell stemness in doxorubicin-resistant breast cancer cells. *Oncotarget* **5**, 70521–70537 (2017).
58. A. Khatib *et al.*, The glutathione peroxidase 8 (GPX8)/IL-6/STAT3 axis is essential in maintaining an aggressive breast cancer phenotype. *Proc. Natl. Acad. Sci. U.S.A.* **117**, 21420–21431 (2020).
59. J. Kreuger, L. Kjellén, Heparan sulfate biosynthesis. *J. Histochem. Cytochem.* **60**, 898–907 (2012).
60. M. Xie, J. Li, Heparan sulfate proteoglycan – A common receptor for diverse cytokines. *Cell Signal* **54**, 115–121 (2019).
61. S. Yamada *et al.*, Embryonic fibroblasts with a gene trap mutation in Ext1 produce short heparan sulfate chains*. *J. Biol. Chem.* **279**, 32134–32141 (2004).
62. T. Wu *et al.*, clusterProfiler 4.0: A universal enrichment tool for interpreting omics data. *Innovation* **2**, 100141 (2021).
63. M. Dai *et al.*, Evolving gene/transcript definitions significantly alter the interpretation of GeneChip data. *Nucleic Acids Res.* **33**, e175 (2005).
64. D. P. Cook, B. C. Vanderhyden, Context specificity of the EMT transcriptional response. *Nat. Commun.* **11**, 2142 (2020).
65. D. van Dijk *et al.*, Recovering gene interactions from single-cell data using data diffusion. *Cell* **174**, 716–729.e27 (2018).